

AD-A186 160

SOLAR TIDES IN THE UPPER EQUATORIAL THERMOSPHERE: A  
COMPARISON BETWEEN RE. (U) AIR FORCE INST OF TECH  
WRIGHT-PATTERSON AFB OH M F STORZ 1987

1/1

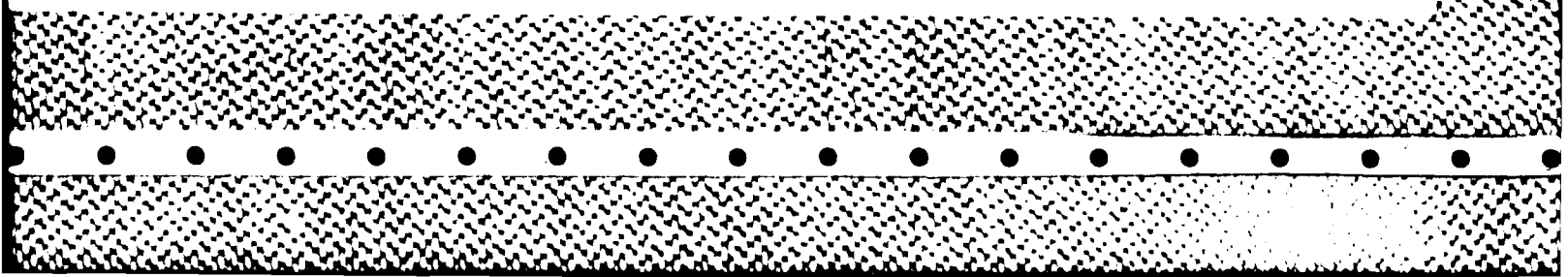
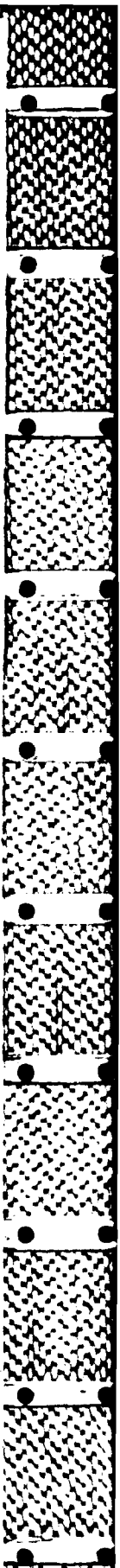
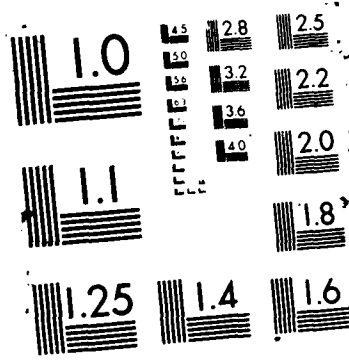
UNCLASSIFIED

AFIT/CI/NR-87-113T

F/G 4/1

NL


1/1  
1/1  
1/1



UNCLASSIFIED

SECURITY CLASSIFICATION OF THIS PAGE (When Data Entered)

REPORT DOCUMENTATION PAGE

READ INSTRUCTIONS BEFORE COMPLETING FORM

REPORT NUMBER  
AFIT/CI/NR 87-113T

2. GOVT ACCESSION NO.  
*File 50*

3. RECIPIENT'S CATALOG NUMBER

4. TITLE (and Subtitle)  
Solar Tides in the Upper Equatorial Thermosphere:  
A Comparison Between AE-E Data and the NCAR  
Thermospheric General Circulation Model

5. TYPE OF REPORT & PERIOD COVERED

THESIS/DISSERTATION

6. PERFORMING ORG. REPORT NUMBER

7. AUTHOR(s)

Mark F. Storz

8. CONTRACT OR GRANT NUMBER(s)

9. PERFORMING ORGANIZATION NAME AND ADDRESS

AFIT STUDENT AT:  
University of Michigan

10. PROGRAM ELEMENT, PROJECT, TASK AREA & WORK UNIT NUMBERS

11. CONTROLLING OFFICE NAME AND ADDRESS

AFIT/NR  
WPAFB OH 45433-6583

12. REPORT DATE  
1987

13. NUMBER OF PAGES  
16+

14. MONITORING AGENCY NAME & ADDRESS (if different from Controlling Office)

15. SECURITY CLASS. (of this report)

UNCLASSIFIED

15a. DECLASSIFICATION/DOWNGRADING SCHEDULE

16. DISTRIBUTION STATEMENT (of this Report)

APPROVED FOR PUBLIC RELEASE; DISTRIBUTION UNLIMITED

**DTIC ELECTED**  
**S** **D**  
NOV 18 1987  
CED

17. DISTRIBUTION STATEMENT (of the abstract entered in Block 20, if different from Report)

18. SUPPLEMENTARY NOTES

APPROVED FOR PUBLIC RELEASE: IAW AFR 190-1

*Lynn E. Wolaver*  
LYNN E. WOLAVER 25 SEP 87  
Dean for Research and  
Professional Development  
AFIT/NR

19. KEY WORDS (Continue on reverse side if necessary and identify by block number)

20. ABSTRACT (Continue on reverse side if necessary and identify by block number)

ATTACHED

AD-A186 160

MMIC FILE COPY

1

Solar Tides in the Upper Equatorial Thermosphere :  
A Comparison Between AE-E Data and the NCAR  
Thermospheric General Circulation Model

by  
Mark F. Storz

This report was submitted  
in partial fulfillment of the requirements for the degree of  
Master of Science  
(Atmospheric Science)  
in the University of Michigan  
1987

Academic Advisor: Professor Vincent J. Abreu

This report has been submitted for publication in  
*Planetary Science and Space Physics*



Accession For	
NIS CRA&I	<input checked="" type="checkbox"/>
DTIC TAB	<input type="checkbox"/>
Unannounced	<input type="checkbox"/>
Justification	
By	
Date	
Security Index	
Availability Codes	
Avail and/or	
Statement	
A-1	

# Solar Tides in the Upper Equatorial Thermosphere : A Comparison Between AE-E Data and the NCAR Thermospheric General Circulation Model 1. Solstice

M. F. STORZ AND V. J. ABREU

*Space Physics Research Laboratory, Ann Arbor, Michigan*

C. G. FESEN

*Laboratory for Atmospheric and Space Physics, University of Colorado, Boulder, Colorado*

Numerical calculations of the equatorial thermospheric tidal temperatures and densities are compared with mass spectrometer data from the Atmosphere Explorer-E satellite (AE-E) for solar minimum solstice conditions. The model calculations were made using the National Center for Atmospheric Research thermospheric general circulation model (TGCM), which includes the effects of viscosity, conductivity, diffusion, ion drag, winds, and temperature gradients. The thermospheric diurnal and semidiurnal tides are excited in situ by solar heating and by ion-neutral momentum coupling. The semidiurnal tidal calculations also include the effects of upward propagating waves generated by heating in the lower atmosphere. The semidiurnal propagating component is modeled by use of the classical tidal perturbations as lower boundary conditions. The model has been tuned by adjusting the propagating tidal forcing term until calculated semidiurnal winds and temperature fields best approximate incoherent scatter observations. The TGCM reproduces the gross tidal features, including the nighttime maxima. The largest discrepancy is the relative weakness of the model's diurnal amplitudes. This may be due to uncertainties in the EUV heating rates and thermospheric cooling rates. On the other hand, the model semidiurnal density amplitudes are considerably larger than those of the data. The terdiurnal amplitudes match fairly well, but the data exhibit a greater asymmetry about the geographic equator.

## INTRODUCTION

In the equatorial thermosphere, the greatest variations in bulk motion, temperature, pressure and densities are solar tides driven either directly or indirectly by the daily variation of solar heating. Because of their importance in understanding the dynamics and chemistry of the thermosphere, solar tides have been the subject of much experimental and theoretical study. Fourier decomposition of the local solar time (LST) variation of satellite-observed neutral densities and temperatures can be used to isolate the diurnal, semidiurnal, and terdiurnal components of the solar tide. Each of these components is discussed more fully below. The three major mechanisms responsible for driving solar tides in the thermosphere are: in situ solar extreme ultraviolet (EUV) heating, ion-neutral momentum coupling, and upward propagating tides.

The most important energy source is in situ EUV heating. Photoionization of atomic oxygen by wavelengths shorter than 103 nm is the absorption process chiefly responsible for the heating of the upper thermosphere. The potential energy gained by the  $O^+$  ions is the major immediate source for heating of the neutral gas via recombination reactions [Massey and Bates, 1982]. A rise in temperature causes the thermosphere to expand resulting in greater column densities, hence greater number densities, at a given altitude. Therefore, in the absence of wind-induced diffusion, these thermospheric densities increase with temperature.

Another important mechanism for tidal fluctuations is ion-neutral momentum coupling. In the absence of collisions, ions are constrained to the earth's magnetic field lines. Therefore, collisions with ions generally inhibit the zonal flow of neutral gas. Since the ion density is generally greater in the daytime, obstruction of the zonal flow of neutral gas is also greater. At night, the neutral gas is relatively free to rush into the lower pressure of the nighttime thermosphere. The resulting adiabatic compression produces a localized nighttime temperature and pressure bulge [Mayr *et al.*, 1974; Spencer *et al.*, 1979]. In the daytime thermosphere, the neutral gas flows away from the high pressure associated with the afternoon temperature maximum. This flow is inhibited by the greater daytime ion densities thus suppressing the adiabatic cooling that normally occurs in a divergent flow. The net result is a semidiurnal fluctuation with two temperature maxima; one appears as an enhancement of the afternoon temperature maximum and the other appears as the nighttime temperature maximum.

The third major source of tidal fluctuations in the thermosphere is the propagation of tides from the lower atmosphere. These upward propagating tides originate from heating due to ozone absorption of UV flux in the mesosphere and  $H_2O$  absorption in the troposphere and lower

stratosphere. Because of their longer vertical wavelengths, the semidiurnal tides are the most significant of the upward propagating tides in the thermosphere [*Hong and Lindzen, 1976*].

### *Diurnal*

The diurnal tide is the dominant thermospheric tidal component. It is excited mainly by in situ absorption of solar EUV radiation with modification by ion-neutral momentum coupling. However, from about 90 to 150km, there is approximately equal contribution from in situ and upward propagating components. The propagating diurnal modes are confined to  $\pm 30^\circ$  latitude; however, these modes generally have small vertical wavelengths leading to destructive interference [*Lindzen, 1966*]. Therefore, the diurnal response is largely confined to the region of excitation within the thermosphere. The (1,1) propagating mode, however, transports energy upwards, reaching a maximum at about 110 km above which it is rapidly dissipated. The diurnal temperature maximum occurs at about 1600 LST and is nearly constant with latitude and altitude above 200km. The phase of the diurnal density maximum should be very similar to that of the diurnal temperature in the absence of adiabatic heat transfer in the thermosphere. However, empirical studies have shown that the diurnal component of total density has an earlier maximum at 1400 LST [*Jacchia et al., 1973; Broglio et al., 1976*]. This phase difference between the diurnal temperature and density maxima has been attributed to the adiabatic heating associated with the large-scale thermospheric circulation [*Dickinson et al., 1968; Volland and Mayr, 1970*]. The phase of the diurnal maximum of atomic oxygen, the major constituent, is shifted to an earlier local time due to wind-induced diffusion. Therefore, atomic oxygen is not in diffusive equilibrium in the lower thermosphere [*Mayr and Volland, 1972*]. Further, mass spectrometer data from OGO-6 [*Hedin et al., 1973*] and San Marco 3 [*Newton et al., 1973*] demonstrated that each neutral constituent has a different diurnal maximum phase.

### *Semidiurnal*

The semidiurnal tide predominates in the lower thermosphere from about 100 to 150 km. At higher altitudes, the diurnal tide dominates. The semidiurnal tide is attributed to three sources: in situ EUV heating, in situ ion-neutral momentum coupling, and upward propagating tides from below. Since these upward propagating tides depend on the dynamics of the lower atmosphere, the semidiurnal tide is more variable than the diurnal tide. The (2,2), (2,3), (2,4), and (2,5) modes all contribute to the semidiurnal response, with the (2,2) mode dominating, particularly above 200km. In classical tidal theory, i.e., with no dissipation, temperature gradients, or mean winds, these modes grow exponentially with height. However, in the real thermosphere, the amplitudes and phases are

modified by molecular viscosity, thermal conductivity, and ion drag above about 100 km, causing the amplitudes and phases to asymptote to constant values above about 150-200 km [Hong and Lindzen, 1976; Forbes, 1982]. Background winds and temperature gradients generate additional tidal components due to mode coupling, in which energy cascades from lower to higher order modes [Lindzen and Hong, 1974]. Ion-neutral momentum coupling can produce a similar cascading effect [Mayr et al., 1979].

Altitude profiles of the semidiurnal tide have been obtained from ground-based incoherent scatter data [Fontanari and Alcayde, 1974; Wand, 1976], from rockets [Newton and Mayr, 1973], and from satellites [Newton et al., 1975; Broglio et al., 1976; Sharp et al., 1978; Forbes and Marcos, 1979]. Herrero et al., 1983 observed that the semidiurnal component of temperature is more dominant in the winter hemisphere of the equatorial thermosphere. They have suggested that in situ EUV heating produces a semidiurnal component that is in phase (out of phase) with the ion drag-induced component in winter (summer).

### *Terdiurnal*

The thermospheric terdiurnal tide was observed through incoherent scatter data [Salah and Evans, 1973] and in satellite mass spectrometer data [Hedin et al., 1974]. The terdiurnal tides may arise through nonlinear interaction between the diurnal and semidiurnal tides through ion-neutral momentum coupling. This mechanism may also generate higher order components all of which have minima near 0000 LST [Mayr et al., 1979]. Therefore, this mechanism may help explain the observed equatorial midnight temperature maximum [Spencer et al., 1979]. In the equatorial thermosphere, the terdiurnal temperature component was shown to be as strong as the semidiurnal component in the summer hemisphere, but negligible in the winter hemisphere [Herrero et al., 1983]. The strong summer terdiurnal tide may be due to the fact that the summer EUV heating resembles a square wave which is composed of odd harmonics [Mayr et al., 1974].

In this paper, tidal variations in neutral temperature and densities observed by the Atmosphere Explorer-E satellite (AE-E) are compared to those generated by the National Center for Atmospheric Research (NCAR) Thermospheric General Circulation Model (TGCM) [Dickinson et al., 1981]. The TGCM is a three-dimensional finite-difference model which solves the pressure coordinate primitive equations from an altitude of 97 to 500km. Although many of the mechanisms proposed to explain real tidal phenomena in the thermosphere have been included in the TGCM, various approximations and simplifications have been made. The only tides that are treated as input parameters are the upward propagating semidiurnal Hough modes: (2,2), (2,3), (2,4), and (2,5). These are introduced

as forcing terms on the lower boundary. Other propagating tides such as the (1,1) mode or the various terdiurnal modes were not input to the model, but can arise internally as the model is integrated with time. The major part of the diurnal tide is specified indirectly through the diurnal nature of the solar EUV heat input. Part of the semidiurnal tide is also specified indirectly through the solar EUV heat input.

Neutral temperatures and densities collected by mass spectrometers aboard the Atmosphere Explorer-E satellite (AE-E) are used in this comparison. The neutral temperatures were measured by the neutral atmosphere temperature experiment (NATE) [Spencer *et al.*, 1973]. The neutral densities were obtained from two instruments: the open-source mass spectrometer (OSS) [Nier *et al.*, 1973] and the neutral atmosphere composition experiment (NACE) [Pelz *et al.*, 1973].

The various tidal features revealed in the data are compared to those of the TGCM in order to evaluate the incorporation of tides into this model. This is done by decomposing the tidal fluctuations into their first three Fourier components and displaying them in maps for various layers in the thermosphere. The graphic representation of these tides is done in an identical manner for both the data and the TGCM output. In addition, the geophysical conditions simulated in the model match those of the data.

Here, we will focus on solstice seasons of the minimum phase of the 11-year solar cycle during geomagnetically quiet conditions ( $K_p < 3$ ). The period covered is from the start of northern hemisphere (N.H.) winter 1975/1976 through the end of N.H. winter 1977/1978. The tidal components of neutral temperature, atomic oxygen number density [O] and molecular nitrogen number density [ $N_2$ ] are analyzed.

## NUMERICAL MODEL

The NCAR TGCM is well-documented in the literature [Dickinson *et al.*, 1981, 1984; Robel *et al.*, 1982]. Therefore, only a brief description is given here. The TGCM is a three-dimensional finite-difference model which includes the effects of molecular viscosity and diffusion, thermal conductivity, ion drag, and absorption of UV and EUV solar radiation. The model solves the pressure-coordinate primitive equations for eastward and northward momentum, and the thermodynamic, hydrostatic, and continuity equations. Solutions are therefore obtained for the zonal, meridional, and vertical winds, the geopotential height, perturbation temperature, and neutral densities. These are symbolized by  $u$ ,  $v$ ,  $w$ ,  $\Phi$ ,  $T$ , [O], and [ $N_2$ ], respectively. The calculations are carried out over 24 spherical shells ranging from 97 to 500 km. The horizontal resolution is  $5^\circ$

latitude by  $5^\circ$  longitude. The vertical resolution is one-half a vertical scale height. The upper boundary conditions are zero flux conditions, i.e.  $du/dz = dv/dz = dT/dz = 0$ . At the lower boundary, the  $u$ ,  $v$ ,  $w$ ,  $T$ , and  $\Phi$  fields are specified to be the solutions of the classical tidal equations. This incorporates the effects of the tidal components generated in the lower atmosphere propagating upwards into the thermosphere as described by Fesen et al., 1986.

The TGCM solves for perturbation temperatures and perturbation number densities about global mean values specified by the MSIS-83 model thermosphere [Hedin, 1983]. The ion-drag term is specified by the International Reference Ionosphere IRI-74 [Rawer, 1981]. The UV and EUV solar fluxes are from Hinteregger, 1981. The model was run for solar minimum, geomagnetically quiet, northern hemisphere winter conditions with a solar 10.7-cm flux of 80. Table 1 presents a list of the model input parameters.

The TGCM includes mechanisms which drive solar diurnal, semidiurnal, and terdiurnal tides. The time-dependent heating by absorption of the UV and EUV solar radiation generates the in situ components of the diurnal, semidiurnal, and terdiurnal tides. As mentioned before, this is the dominant source of the diurnal tide. The semidiurnal tide is also excited by in situ ion-neutral momentum coupling and by upward propagating tides from the lower atmosphere. In situ solar heating plays a lesser role in the generation of the semidiurnal tide. The propagating semidiurnal tides are parameterized by an additional forcing term applied to the lower boundary at 97km. This forcing term is adjusted by iterating until the best possible agreement is obtained between the model predictions and incoherent scatter observations [Fesen et al., 1986]. The semidiurnal components included in the TGCM are the (2,2), (2,3), (2,4), and (2,5) modes. The amplitudes and phases of the geopotential height at the lower boundary for these modes are listed in Table 2.

## DATA ANALYSIS

Most studies of thermospheric tides deal with the altitude dependence of these tides. This study focuses on their latitude dependence within a layer roughly corresponding to altitudes from 250 to 290 km. The altitude range is determined by the satellite orbit which varied over this range during the observation period. The thermosphere is nearly isothermal over this altitude range, particularly near solar minimum. Therefore, temperature data from this altitude range may be averaged together without correcting for lapse rate. The approximate range of latitudes covered by AE-E was from  $-20^\circ$  to  $+20^\circ$ . Since each solstice season is three months long, data within 46 days of the dates of solstice were used in this study. Therefore, data measured between Julian day 126 and day 220 are June solstice data and data measured between day 310 and day 36 of the following year are December

solstice data. The June solstice data were inverted about the geographic equator and merged with December solstice data to improve statistics and suppress hemispheric differences. Therefore, the summer hemisphere is the lower half on all maps.

During the minimum phase of the 11-year solar cycle, the EUV heating and its day-to-day fluctuations are at a minimum. Therefore, solar minimum conditions introduce less scatter in the data for a particular latitude and LST. The solar declination does not vary as much during solstice seasons as it does for equinoxes. Therefore, all data for a solstice-centered three month period represent similar seasonal conditions.

Contour maps of the various quantities were made using geographic latitude as the meridional coordinate and local solar time (LST) as the zonal coordinate. Each map is decomposed into the first three Fourier components: the diurnal, semidiurnal and terdiurnal tides. These different components are also represented as contour maps using the same meridional and zonal coordinates. When this is done, both phase and amplitude information can be represented on a single diagram.

Before maps of the temperature and densities can be created, the data must be sorted into bins having different local solar times and geographic latitudes. The dimensions of each bin are 2 hours LST by  $10^\circ$  latitude. These bins are overlapped by 1 hour LST in the zonal direction and by  $5^\circ$  latitude in the meridional direction. This serves to increase the resolution of the binning scheme without seriously lowering the number of data points collected in any particular bin. This binning scheme has 7 rows of bins corresponding to different latitudes and 24 columns of bins corresponding to different local solar times making a total of 168 bins.

Prior to binning, each measured temperature was divided by the mean temperature of the equatorial thermosphere for that day. This normalization greatly reduces scatter in the data due to solar cycle changes in the mean temperature. The mean temperature ranged from 690 K to 920 K during the data period. Since the amplitude of the diurnal temperature fluctuation is roughly proportional to the mean temperature [Herrero *et al.*, 1983], the scatter introduced by solar cycle changes in the diurnal amplitude was also reduced. Since it takes AE-E approximately 48 days to cover all local solar times and equatorial latitudes, one day of temperature observations is insufficient for calculating a reliable mean temperature. In order to eliminate changes in the mean temperatures related to solar rotation, a period equivalent to two solar rotations (55 days) was chosen as the time interval over which this mean was calculated. This time interval is centered on the date of the data being normalized. Only geomagnetically quiet ( $K_p < 3$ ) temperature data were used in the calculation of these mean temperatures. Multiplying the binned normalized temperatures by the mean

temperature of the thermosphere for the entire observation period converts them to temperature values. This procedure reduces the typical standard deviation for each bin from ~70 K to ~35 K which greatly improves the confidence in the features appearing in the contour maps.

A similar normalization procedure was applied to the observed neutral densities. A 55-day running mean was calculated for the altitude of the reference density at the midpoint of the density layer. The density layer for atomic oxygen is  $\log_{10}[\text{O}] = 8.80 \pm 0.20$ ; the layer for molecular nitrogen is  $\log_{10}[\text{N}_2] = 8.20 \pm 0.35$ . The value in brackets is the number density measured in  $\text{cm}^{-3}$ . Because of the different molecular weights of the two species, different density ranges were needed to cover the same altitude range. These reference densities were chosen to correspond to approximately 270 km on the average. As with the mean temperature values, the reference altitudes ( $Z_{\text{ref}}$ ) were calculated using geomagnetically quiet data and averaged over all equatorial latitudes and local solar times for the observed layer. The densities measured at the satellite altitude ( $Z_{\text{sat}}$ ) were then normalized to the reference altitudes by use of the hydrostatic equation in the form:

$$[M]_{\text{normalized}} = [M]_{\text{measured}} \exp(\Delta Z/H),$$

where  $\Delta Z = Z_{\text{sat}} - Z_{\text{ref}}$  and  $H$  is the scale height of the particular species  $[M]$  being normalized. Since the scale height is temperature-dependent, normalizing the neutral density data required neutral temperature to be available. Consequently, the satellite data were restricted to those which simultaneously measured temperatures and densities.

The molecular nitrogen reference density level was chosen so as to have an average altitude similar to that of the atomic oxygen reference density level. However, because of the different scale heights of the two species, the reference altitudes for a particular day differ in general. Near solar minimum, the mean altitude of the atomic oxygen reference density level is lower (248 km) than the corresponding molecular nitrogen density level (256 km). As solar maximum is approached, the oxygen level becomes higher (294 km) than the nitrogen level (287 km). These altitude ranges are greater than one scale height of the associated species. Therefore, there is considerably less scatter in the densities normalized to these fluctuating mean altitudes than there would be if both densities were normalized to one fixed altitude.

After sorting, a four-point quadratic least squares fit was applied in both zonal and meridional directions. This is numerically equivalent to fitting a two-dimensional second-order polynomial function of the form:  $f(x,y) = a_0 + a_1x + a_2y + a_3xy + a_4x^2 + a_5y^2 + a_6x^2y + a_7xy^2 + a_8x^2y^2$  to 16 bins at a time. The least squares fit was done in an integral sense: the quantity minimized was the

difference between the double integral of the polynomial over a particular bin and the average data value of that bin. Adjacent solutions generated in this way were blended together using a cosine weighting function. The resulting smoothed arrays are used to generate contour maps of the neutral densities and temperatures with geographic latitude and local solar time as the map coordinates.

The tidal fluctuations presented in this study are the diurnal, semidiurnal, and terdiurnal components. The un-decomposed maps of the neutral atmospheric quantities studied in this paper are compared to the TGCM in Figure 1 and to MSIS-86 in Figure 2. MSIS-86 is an empirical model for the neutral temperature and constituents of the thermosphere [Hedin, 1987]. The un-decomposed maps are the original maps not subject to any Fourier decomposition. These maps may be viewed as a natural superposition of all tidal components, including the zonal mean. Maps of neutral temperature  $T$  are in the top row, atomic oxygen number density  $[O]$  is in the middle row, and molecular nitrogen number density  $[N_2]$  is in the bottom row. Maps of the data from AE-E are in the left-hand column and maps of model output are in the right-hand column. Corresponding maps of AE-E data and model output are displayed in precisely the same manner to facilitate comparison. The tidal maps (Figures 3, 4, and 5) are contour maps of the diurnal, semidiurnal, and terdiurnal tides respectively. Each map exhibits both phase and amplitude information for each of the respective tides. The position of each wavecrest is marked by a heavy line extending along the ridges from top to bottom of each map. There are two ridge lines in the maps of the semidiurnal component (Figure 4) and three ridge lines in the maps of the terdiurnal component (Figure 5). The position of these ridge lines in LST is the phase of the tidal component. Most studies only graph the phase of the wavecrest closest to 0000 LST, since the other wavecrests are parallel to it.

The other lines on each map are contour lines. In the temperature maps, a contour interval of 10 K was used in the un-decomposed maps (Figures 1 and 2) and the maps of the diurnal component (Figure 3). A contour interval of 5 K was used in the maps of the semidiurnal component (Figure 4) and the maps of the terdiurnal component (Figure 5). In the density maps,  $\log_{10}$  of the number density is contoured. Therefore, for a contour interval of 0.02, each successively higher contour represents an increase in the number density by a factor of  $10^{0.02} = 1.0471$  or a 4.71% increase. Such a contour interval is used in the un-decomposed maps and the maps of the diurnal components. In the maps of the semidiurnal component and the terdiurnal component, a contour interval of 0.01 is used.

## COMPARISON

Here we will discuss the similarities and differences between the NCAR TGCM and the AE-E

data. In the upper equatorial thermosphere, this model reproduces the gross features of the tides observed in the AE-E data. In addition, it reproduces nighttime maxima in T, [O], and [N<sub>2</sub>]. However, there are several important discrepancies.

In the un-decomposed contour maps (Figure 1), the LST of minima and maxima generally agree for all three quantities studied. The temperature and N<sub>2</sub> density data exhibit broader maxima in the summer hemisphere, whereas the model has broad less defined maxima at all latitudes. In the case of atomic oxygen, the model actually has two weak daytime maxima at 11 hrs and 15 hrs LST. In the maps of AE-E temperature, the summer hemisphere has a much steeper drop after the afternoon maximum than the morning rise in temperature. More symmetrical temperature gradients occur in the winter hemisphere. This characteristic, which is reflected in the N<sub>2</sub> density, was also noted by Herrero et al., 1983. The TGCM has similar temperature gradients in both hemispheres. In the atomic oxygen map, the AE-E data shows a better defined maximum which is greatest at +10° latitude.

A set of un-decomposed maps showing the agreement between the data and the MSIS-86 empirical model are shown in Figure 2. There is generally good agreement between the data and MSIS-86 for all three quantities, especially neutral temperature. In the [O] maps, the data show a *stronger afternoon maximum in the winter hemisphere* whereas MSIS-86 favors the summer hemisphere. In the [N<sub>2</sub>] maps, the AE-E data show a morphology similar to that of the neutral temperature with a broader afternoon maximum in the summer hemisphere. MSIS-86, however, exhibits a broader afternoon maximum in the winter hemisphere. The nighttime maxima are better defined in the data than in MSIS-86.

The TGCM generally exhibits less latitudinal structure than the data. However, in the evening sector (18-24hrs LST), the TGCM shows a significant latitudinal structure in the nighttime temperature and [N<sub>2</sub>] maxima. The data has an even stronger latitudinal structure in these nighttime maxima. In all three data parameters, the AE-E data has a nighttime maximum between 0000 and 0200 LST and between -10° and -15° latitude. The TGCM has nighttime maxima that span both hemispheres and favor the winter hemisphere in the case of temperature and [O].

### *Diurnal*

The comparison between the observed and modelled diurnal tidal components of T, [O], and [N<sub>2</sub>] are shown in Figure 3. The observed temperature and N<sub>2</sub> density phases are 1500-1600 LST, while the [O] phase is earlier at about 1300 LST. The temperature amplitude is about 85 K. The

latitudinal variation is very flat in the equatorial region in agreement with the TGCM. The diurnal components of the MSIS-86 empirical model are very similar to those of the AE-E data.

The TGCM diurnal tide reproduces the morphology to a fair degree, but the magnitudes are quite different. The most obvious difference is the relative weakness of the model amplitudes. The observed diurnal temperature amplitude is about 40% greater than the model, while the observed density amplitudes are roughly double those of the model. The  $[N_2]$  modelled and observed phases agree quite well, with the maxima occurring about 1500 LST, but the model phases of T and [O] are about 2 hours earlier than the observed phases of 1600 and 1300 LST respectively. It is likely that both the EUV heating rate and the thermospheric cooling rate have been underestimated somewhat in the model. To keep the model's mean thermospheric temperature in agreement with the data, the heating rate and the cooling rate should be increased by about the same factor.

### *Semidiurnal*

The comparison between the observed and modelled semidiurnal tide of T, [O], and  $[N_2]$  is shown in Figure 4. The data show maximum phases for all three observed quantities at about 0200 and 1400 LST. The temperature and, to some extent, the  $[N_2]$  tides are stronger in the winter hemisphere. The temperature map in particular appears quite consistent with a predominant (2,3) mode, with possible contributions from the (2,4). This is in agreement with the strong (2,3) nature of the TGCM temperature tide. The  $[N_2]$  semidiurnal tide also shows some evidence of a (2,3) mode. The semidiurnal temperature tide of the MSIS-86 model is in very good agreement with the data. For both densities, the TGCM has amplitudes very similar to those of the MSIS-86. However, unlike the TGCM, the MSIS-86 density tides occur almost exclusively in the summer hemisphere. Both TGCM density maxima are in the winter hemisphere, whereas the AE-E [O] tide favors the summer hemisphere. The TGCM semidiurnal temperature amplitude at the winter edge of the map is 30 K, compared to 25 K for the data. The TGCM  $N_2$  and O density amplitudes are roughly 2 and 2.5 times greater than the data respectively. The model phases are earlier than observed: 4 hours for the temperature, and 1.5-2 hours for the densities.

The modelled amplitudes and phases are more suggestive of the antisymmetric modes, particularly the (2,3). Better agreement may be obtained by decreasing the contribution of the antisymmetric modes in the model. However, since the diurnal tide contributes to the semidiurnal response through ion-neutral coupling, it is important that agreement with the diurnal tide be improved first.

### *Terdiurnal*

The observed and modelled terdiurnal tidal components are shown in Figure 5. Both the observations and the MSIS-86 model exhibit a pronounced asymmetry for T and  $[N_2]$  with stronger tides in the summer hemisphere. However, the AE-E [O] tide, like the TGCM, favors the winter hemisphere. Herrero et al., 1983, also show the terdiurnal temperature amplitude to be stronger in the summer hemisphere of the equatorial region. The model variations are more symmetric, particularly for the densities. The TGCM density amplitudes are in quite good agreement with the data, but the data temperature amplitude of 22 K is 30% greater than the TGCM. The model T and  $[N_2]$  amplitudes peak more towards the winter hemisphere, unlike the data. The TGCM phases are constant with latitude, whereas the observations show significant phase shifts between  $+10^\circ$  and  $+20^\circ$ . The terdiurnal tides are generated in the model through coupling with the diurnal and semidiurnal tides. Therefore, improving the agreement for the diurnal and semidiurnal tides may result in better agreement for the terdiurnal component.

### *Difference Maps*

Difference maps produced by subtracting the AE-E amplitudes and phases from those of the TGCM are shown in Figures 6 and 7. The left-hand column of Figure 6 shows the contour maps obtained when the AE-E data are subtracted from the TGCM output; the right-hand column shows the result of subtracting the data from the model for the diurnal component. Similarly, Figure 7 shows the data subtraction from the model for the semidiurnal and terdiurnal components. These illustrate the various discrepancies noted above. The difference diurnal and semidiurnal components indicate that for all three quantities, the discrepancy is greater in the winter hemisphere. However, the discrepancies in the terdiurnal components are greater in the summer hemisphere.

### CONCLUSION

The Atmosphere Explorer-E satellite (AE-E) had a sufficiently dense data coverage to provide a solid test of the accuracy of the NCAR TGCM. The normalization technique used in processing the temperatures and densities greatly reduced the scatter in these data for a particular latitude and local solar time. These data agree very well with the MSIS-86 empirical model except for the semidiurnal and terdiurnal density tides. The MSIS-86  $[N_2]$  and [O] semidiurnal tides are respectively 1.5 and 2.5 times stronger than the AE-E data and, unlike the AE-E data, strongly favor the summer hemisphere. On the other hand, AE-E terdiurnal density tides are about 1.5 times stronger than those of MSIS-86.

The NCAR TGCM is capable of reproducing the gross tidal features of the upper equatorial thermosphere, including the nighttime maxima in  $T$ ,  $[O]$ , and  $[N_2]$ . The most significant discrepancy is the relative weakness of the model's diurnal tidal amplitudes. The AE-E temperature amplitude is about 40% greater than that of the model, while the AE-E density amplitudes are roughly double those of the model. An increase of the EUV heating and thermospheric cooling rates by the same percentage should bring the model into better agreement with the data. For the semidiurnal tides, the major discrepancy is the earlier temperature maximum in the TGCM compared to the data. The observed terdiurnal tides are strongly asymmetric, with maximum amplitudes in the summer hemisphere; the model results are more symmetric and tend to peak in the wrong hemisphere. Improvement of the diurnal tidal results necessitates investigation and possible adjustment of the various heating parameterizations in the TGCM. This will affect the semidiurnal and terdiurnal tides agreement with the data through ion-neutral momentum coupling. The semidiurnal tidal results indicate that the model lower boundary conditions, which are a measure of the energy transported upwards by vertically propagating tides, should be altered.

*Acknowledgments.* This work was supported by the National Science Foundation under grant (to be determined). The authors gratefully thank Jeng H. Yi, Anne K. Smith, and Stanley Solomon (Space Physics Research Laboratory) for reviewing the manuscript and suggesting helpful modifications. We also thank Barbara K. Emery at the National Center for Atmospheric Research for her excellent work in running the NCAR TGCM.

## REFERENCES

- Broglio, L., C. Buongiorno, U. Ponzi, and G. Ravelli, San Marco 3 drag balance results below 320 km altitude in the equatorial atmosphere, *Space Res.*, 16, 203-207, 1976.
- Dickinson, R. E., C. P. Lagos, and R. E. Newell, Dynamics of the neutral thermosphere for small Rossby number motions, *J. Geophys. Res.*, 73, 4299-4313, 1968.
- Dickinson, R. E., E. C. Ridley, and R. G. Robel, A three-dimensional general circulation model of the thermosphere, *J. Geophys. Res.*, 86, 1499-1512, 1981.
- Dickinson, R. E., E. C. Ridley, and R. G. Robel, Thermospheric general circulation with coupled dynamics and composition, *J. Atmos. Sci.*, 41, 205-219, 1984.
- Fesen, C. G., R. E. Dickinson, R. G. Robel, Simulation of the thermospheric tides at equinox with the National Center for Atmospheric Research thermospheric general circulation model, *J. Geophys. Res.*, 91, 4471-4489, 1986.
- Fontanari, J., and D. Alcayde, Observations of neutral temperature tidal-type oscillations in the  $F_1$  region, *Radio Sci.*, 9, 275-280, 1974.
- Forbes, J. M., Atmospheric tides, 2, The solar and lunar semidiurnal components, *J. Geophys. Res.*, 87, 5241-5252, 1982.
- Forbes, J. M., and F. A. Marcos, Tidal variations in total mass density as derived from the AE-E Mesa experiment, *J. Geophys. Res.*, 84, 31-35, 1979.
- Hedin, A. E., H. G. Mayr, C. A. Reber, G. R. Carignan, and N. W. Spencer, A global empirical model of thermospheric composition based on Ogo-6 mass spectrometer measurements, *Space Res.*, 13, 315-320, 1973.
- Hedin, A. E., H. G. Mayr, C. A. Reber, N. W. Spencer, and G. R. Carignan, Empirical model of global thermospheric temperature and composition based on data from the Ogo-6 quadrupole mass spectrometer, *J. Geophys. Res.*, 79, 215-225, 1974.
- Hedin, A. E., A revised thermospheric model based on mass spectrometer and incoherent scatter data: MSIS-83, *J. Geophys. Res.*, 88, 10,170-10,188, 1983.
- Hedin, A. E., MSIS-86 thermospheric model, *J. Geophys. Res.*, 92, 4649-4662, 1987.
- Herrero, F. A., H. G. Mayr, and N. W. Spencer, Latitudinal (seasonal) variations in the thermospheric midnight temperature maximum: a tidal analysis, *J. Geophys. Res.*, 88, 7225-7235, 1983.
- Hinteregger, H. E., Representations of solar EUV fluxes for aeronautical applications, *Adv. Space Res.*, 1, 39-52, 1981.
- Hong, S. S., and R. S. Lindzen, Solar semidiurnal tide in the thermosphere, *J. Atmos. Sci.*, 28, 275-280, 1976.
- Jacchia, L. G., I. G. Campbell, and J. W. Slowey, A study of the diurnal variation in the thermosphere as derived by satellite drag, *Planet. Space Sci.*, 21, 1825-1834, 1973.
- Lindzen, R. S., On the relation of wave behavior to source strength and distribution in a propagating medium, *J. Atmos. Sci.*, 23, 630-632, 1966.

- Lindzen, R. S., and S. S. Hong, Effects of mean winds and horizontal temperature gradients on solar and lunar semidiurnal tides in the atmosphere, *J. Atmos. Sci.*, 31, 1421-1466, 1974.
- Massey, H. S. W., and D. R. Bates, *Applied Atomic Collision Physics, Vol. 1, Atmospheric Physics and Chemistry*, 482 pp., Academic Press, New York, NY, 1982.
- Mayr, H. G., A. E. Hedin, C. A. Reber, and G. R. Carignan, Global characteristics in the diurnal variations of the thermospheric temperature and composition, *J. Geophys. Res.*, 79, 619-628, 1974.
- Mayr, H. G., I. Harris, N. W. Spencer, A. E. Hedin, L. E. Wharton, H. S. Porter, J. C. G. Walker, and H. C. Carlson, Atmospheric tides and the midnight temperature anomaly, *Geophys. Res. Lett.*, 6, 447-450, 1979.
- Mayr, H. G., and H. Volland, Diffusion model for the phase delay between thermospheric density and temperature, *J. Geophys. Res.*, 77, 2359-2367, 1972.
- Newton, G. P., and H. G. Mayr, Diurnal and semidiurnal nitrogen density and temperature variations from thermosphere probe measurements, *J. Geophys. Res.*, 78, 5687-5692, 1973.
- Newton, G. P., D. T. Pelz, and W. T. Kasprzak, Equatorial thermospheric composition and its variations, *Space Res.*, 13, 287-290, 1973.
- Newton, G. P., W. T. Kasprzak, S. A. Curtis, and D. T. Pelz, Local time variation of equatorial thermospheric composition determined by the San Marco 3 NACE, *J. Geophys. Res.*, 80, 2289-2299, 1975.
- Nier, A. O., W. E. Potter, D. R. Hickman, and K. Mauersberger, The open-source neutral-mass spectrometer on Atmosphere Explorer-C, -D, and -E, *Radio Sci.*, 8, 271-276, 1973.
- Pelz, D. T., C. A. Reber, A. E. Hedin, G. R. Carignan, A neutral-atmosphere composition experiment for the Atmosphere Explorer-C, -D, and -E, *Radio Sci.*, 8, 277-285, 1973.
- Rawer, K., *International Reference Ionosphere - IRI74*, Eds. J. V. Lincoln and R. O. Conkright, World Data Center A, NOAA, Boulder, CO, 1981.
- Robel, R. G., R. E. Dickinson, and E. C. Ridley, Global circulation and temperature structure of thermosphere with high-latitude plasma convection, *J. Geophys. Res.*, 87, 1599-1614, 1982.
- Sharp, L. R., D. R. Hickman, C. J. Rice, and J. M. Straus, The altitude dependence of the local time variation of thermospheric density, *Geophys. Res. Lett.*, 5, 261-263, 1978.
- Spencer, N. W., H. B. Niemann, and G. R. Carignan, The neutral-atmosphere temperature instrument, *Radio Sci.*, 8, 284-296, 1973.
- Spencer, N. W., G. R. Carignan, H. G. Mayr, N. B. Niemann, R. F. Theis, and L. E. Wharton, The midnight temperature maximum in the earth's equatorial thermosphere, *Geophys. Res. Lett.*, 6, 444-446, 1979.
- Volland, H., and H. G. Mayr, A theory of the diurnal variations of the thermosphere, *Ann. Geophys.*, 26, 907, 1970.
- Wand, R. H., Semidiurnal tide in the E region from incoherent scatter measurements at Arecibo, *Radio Sci.*, 11, 641-652, 1976.

Julian Date	76356 (December, 21 1976)
F <sub>10.7</sub> (10.7-cm flux)	80 [ $\times 10^{-22}$ Wm <sup>-2</sup> Hz]
Zurich sunspot number	20
Ap index	6
Auroral power	5 gigawatts
Crosstail potential	30 kilovolts
Neutral thermospheric initialization model	MSIS-83 [ <i>Hedin, 1983</i> ]
Ionospheric initialization model	International Reference Ionosphere IRI-74 [ <i>Rawer, 1981</i> ]

Table 1. Input parameters used in running the NCAR TGCM.

HOUGH MODE	AMPLITUDE (geopotential meters)	PHASE (hours LST)
2:2	300	2.0
2:3	300	0.0
2:4	300	3.0
2:5	300	4.0

Table 2. Upward propagating components of the semidiurnal tide applied to the lower boundary (97km) of the TGCM. These modes are expressed as spatial fluctuations of a constant pressure surface in the vertical.

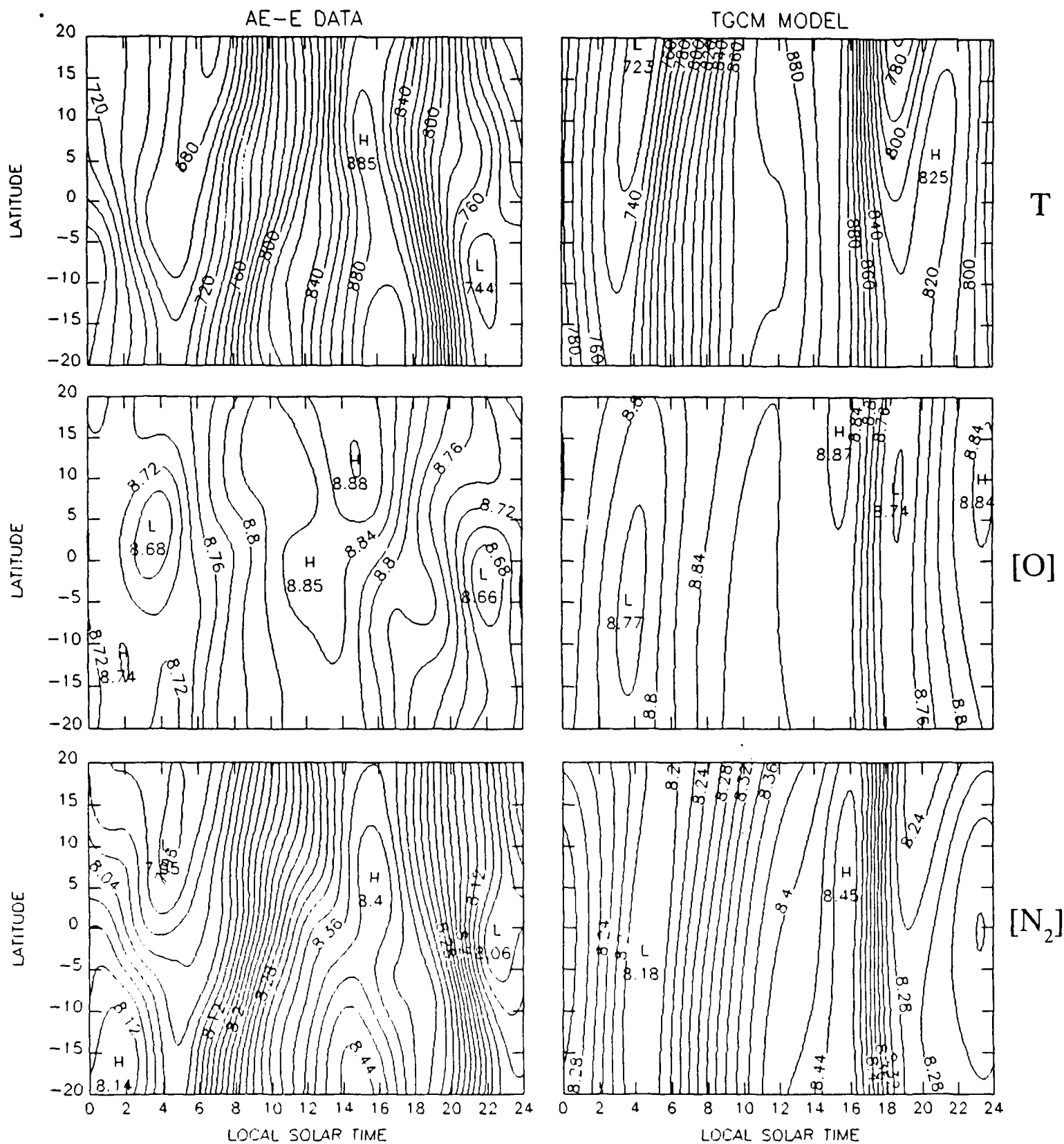


Fig. 1. Un-decomposed maps of T (top row), [O] (middle row), and [N<sub>2</sub>] (bottom row). For the temperature maps, a contour interval of 10 K is used. For the density maps, a contour interval of  $\log_{10}[M] = 0.02$  is used, where [M] is the number density in  $\text{cm}^{-3}$ .

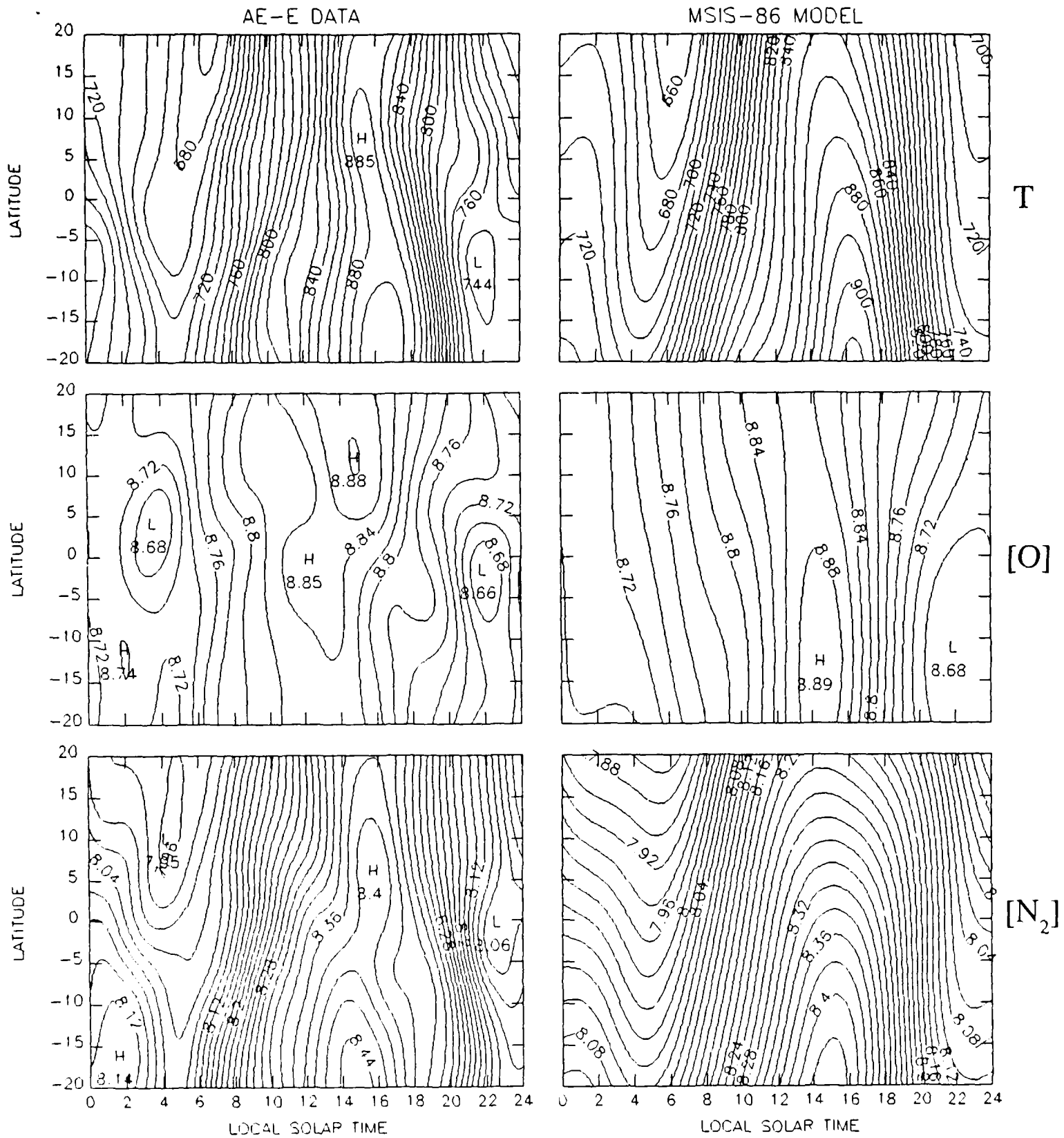


Fig. 2. Same as Fig. 1. except the maps in the right-hand column are from MSIS-86 output.

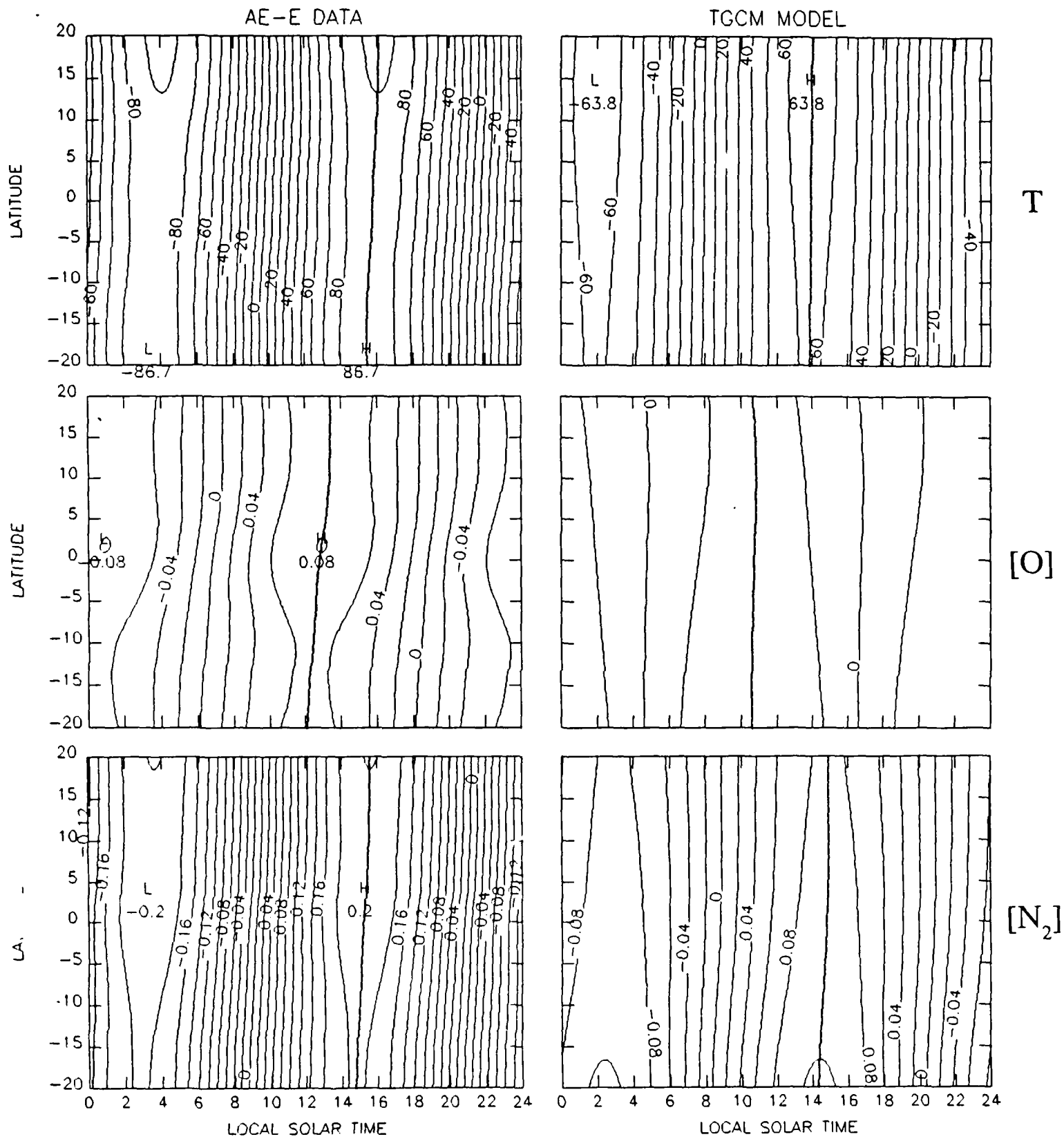


Fig. 3. Diurnal component of T (top row), [O] (middle row), and [N<sub>2</sub>] (bottom row). For the temperature maps, a contour interval of 10 K is used. For the density maps, a contour interval of  $\log_{10}[M] = 0.02$  is used, where [M] is the number density in  $\text{cm}^{-3}$ .

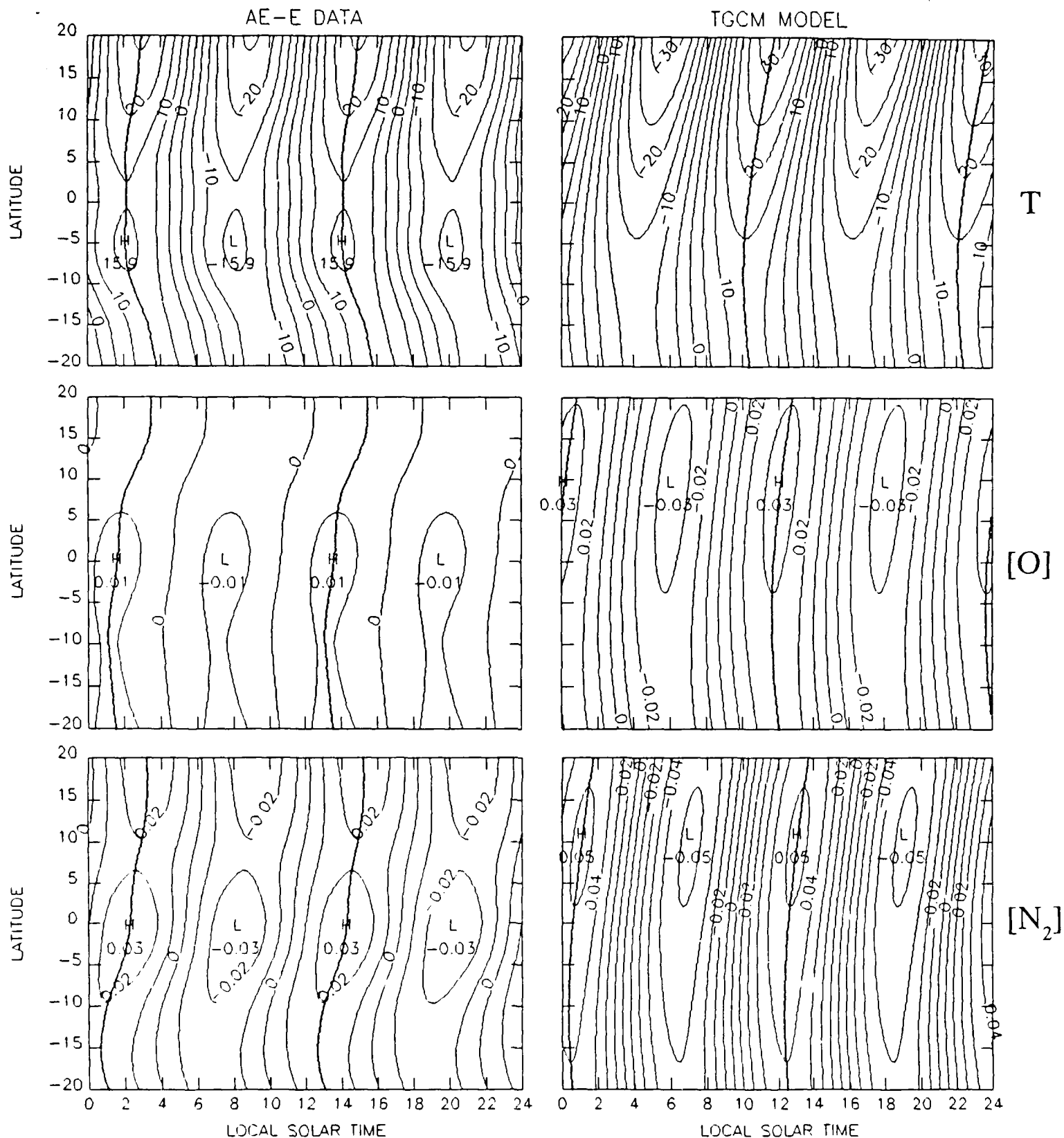


Fig. 4. Semidiurnal component of T (top row), [O] (middle row), and  $[N_2]$  (bottom row). For the temperature maps, a contour interval of 5 K is used. For the density maps, a contour interval of  $\log_{10}[M] = 0.01$  is used, where  $[M]$  is the number density in  $\text{cm}^{-3}$ .

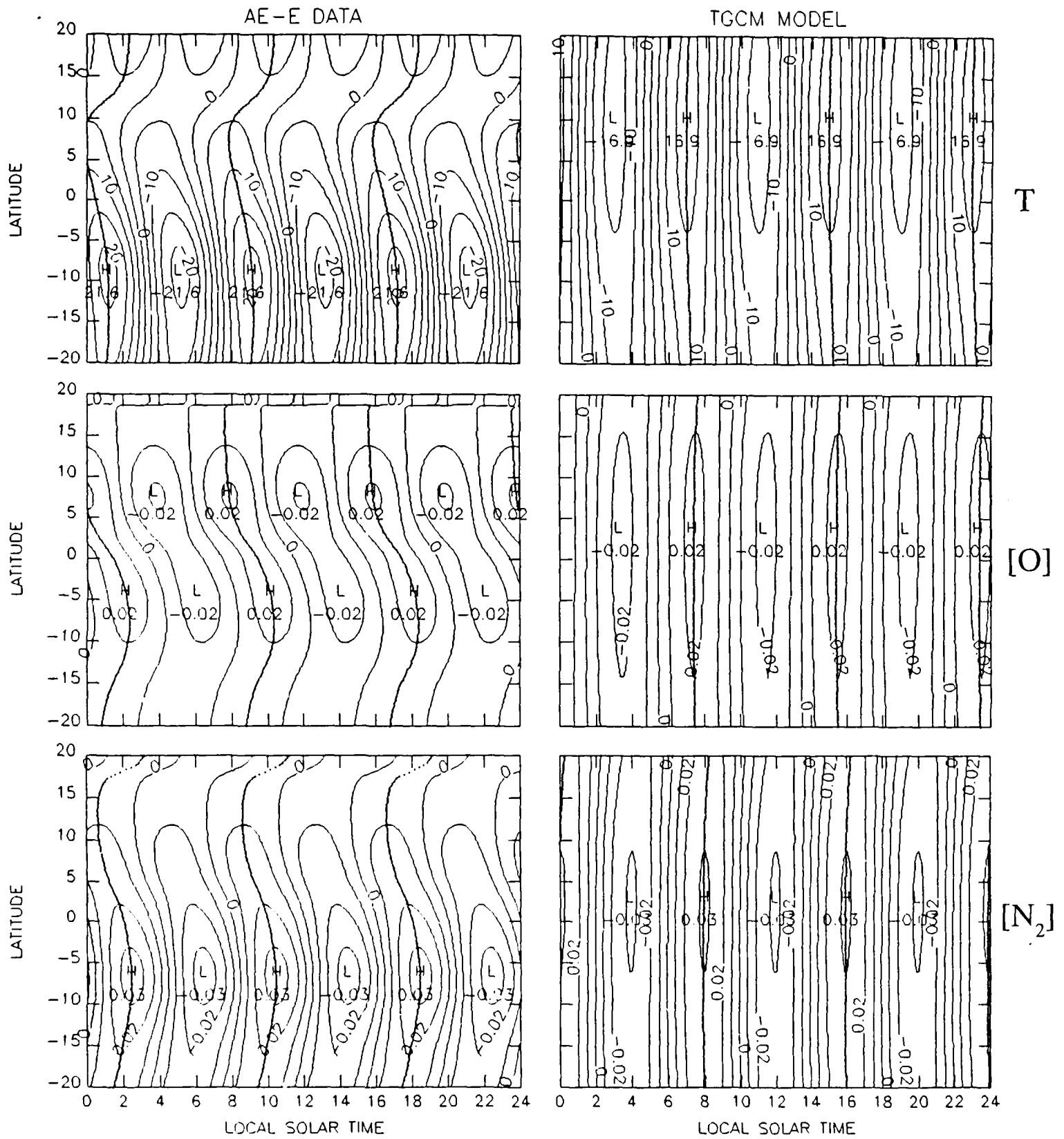


Fig. 5. Terdiurnal component of T (top row), [O] (middle row), and [N<sub>2</sub>] (bottom row). For the temperature maps, a contour interval of 5 K is used. For the density maps, a contour interval of  $\log_{10}[M] = 0.01$  is used, where [M] is the number density in  $\text{cm}^{-3}$ .

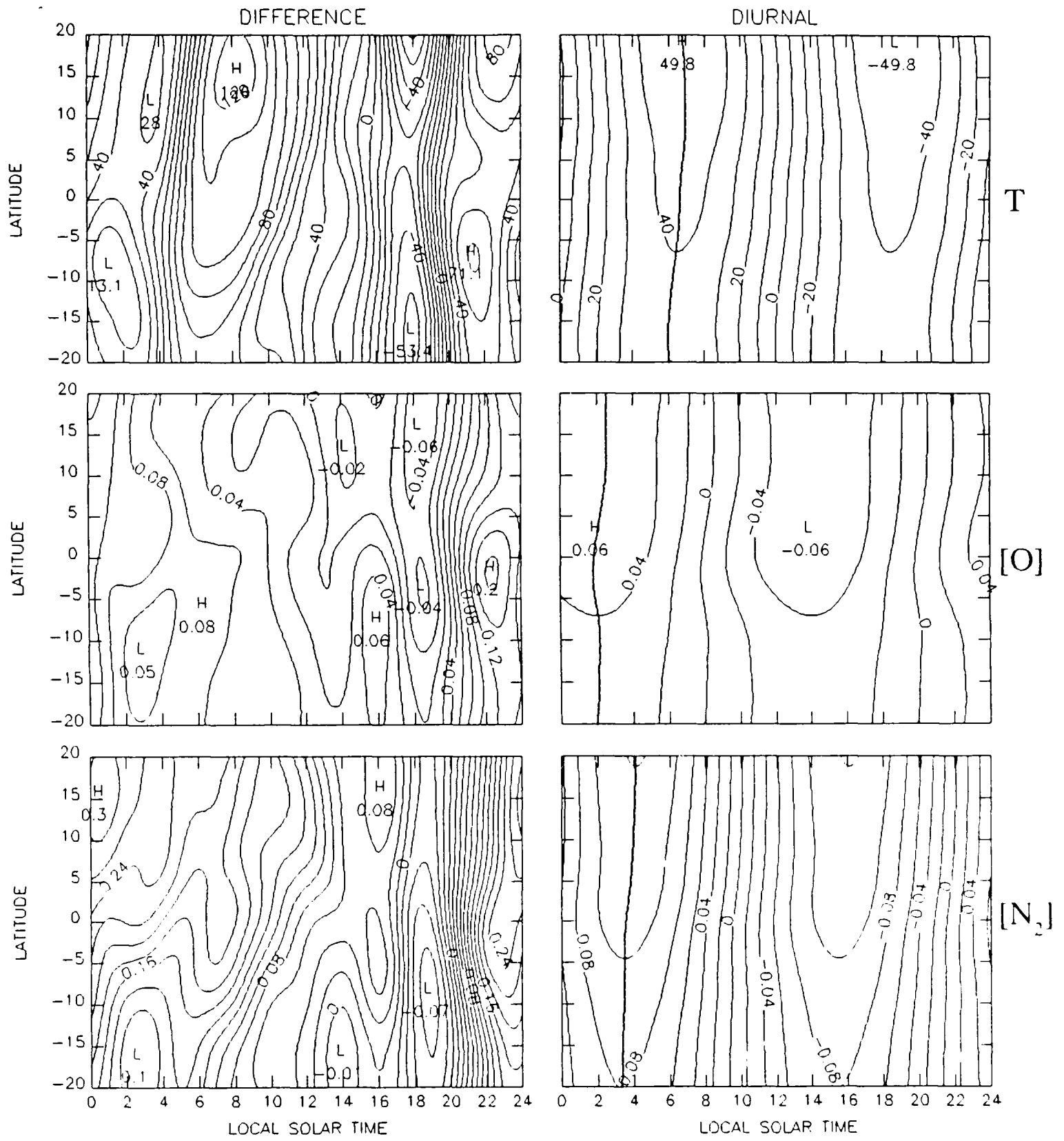


Fig. 6. The difference maps and the difference diurnal components. The AE-E data is subtracted from fields generated by the NCAR TGCM. The contour intervals used are the same as those used in Figures 1, 2, and 3.



Solar Tides in the Upper Equatorial Thermosphere:  
A Comparison Between AE-E Data and the NCAR  
Thermospheric General Circulation Model

by  
Mark F. Storz, Captain, USAF

This report (23 pages) was submitted  
as a requirement for the degree of  
Master of Science  
(Atmospheric Science)  
in the University of Michigan  
1987

# ~~Solar Tides in the Upper Equatorial Thermosphere : A Comparison Between AE-E Data and the NCAR Thermospheric General Circulation Model 1. Solstice~~

~~M. E. STORZ AND V. J. ABREU~~

~~*Space Physics Research Laboratory, Ann Arbor, Michigan*~~

~~C. G. FESEN~~

~~*Laboratory for Atmospheric and Space Physics, University of Colorado, Boulder, Colorado*~~

Numerical calculations of the equatorial thermospheric tidal temperatures and densities are compared with mass spectrometer data from the Atmosphere Explorer-E satellite (AE-E) for solar minimum solstice conditions. The model calculations were made using the National Center for Atmospheric Research thermospheric general circulation model (TGCM), which includes the effects of viscosity, conductivity, diffusion, ion drag, winds, and temperature gradients. The thermospheric diurnal and semidiurnal tides are excited in situ by solar heating and by ion-neutral momentum coupling. The semidiurnal tidal calculations also include the effects of upward propagating waves generated by heating in the lower atmosphere. The semidiurnal propagating component is modeled by use of the classical tidal perturbations as lower boundary conditions. The model has been tuned by adjusting the propagating tidal forcing term until calculated semidiurnal winds and temperature fields best approximate incoherent scatter observations. The TGCM reproduces the gross tidal features, including the nighttime maxima. The largest discrepancy is the relative weakness of the model's diurnal amplitudes. This may be due to uncertainties in the EUV heating rates and thermospheric cooling rates. On the other hand, the model semidiurnal density amplitudes are considerably larger than those of the data. The terdiurnal amplitudes match fairly well, but the data exhibit a greater asymmetry about the geographic equator.

## REFERENCES

- Broglio, L., C. Buongiorno, U. Ponzi, and G. Ravelli, San Marco 3 drag balance results below 320 km altitude in the equatorial atmosphere, *Space Res.*, 16, 203-207, 1976.
- Dickinson, R. E., C. P. Lagos, and R. E. Newell, Dynamics of the neutral thermosphere for small Rossby number motions, *J. Geophys. Res.*, 73, 4299-4313, 1968.
- Dickinson, R. E., E. C. Ridley, and R. G. Robel, A three-dimensional general circulation model of the thermosphere, *J. Geophys. Res.*, 86, 1499-1512, 1981.
- Dickinson, R. E., E. C. Ridley, and R. G. Robel, Thermospheric general circulation with coupled dynamics and composition, *J. Atmos. Sci.*, 41, 205-219, 1984.
- Fesen, C. G., R. E. Dickinson, R. G. Robel, Simulation of the thermospheric tides at equinox with the National Center for Atmospheric Research thermospheric general circulation model, *J. Geophys. Res.*, 91, 4471-4489, 1986.
- Fontanari, J., and D. Alcayde, Observations of neutral temperature tidal-type oscillations in the  $F_1$  region, *Radio Sci.*, 9, 275-280, 1974.
- Forbes, J. M., Atmospheric tides, 2, The solar and lunar semidiurnal components, *J. Geophys. Res.*, 87, 5241-5252, 1982.
- Forbes, J. M., and F. A. Marcos, Tidal variations in total mass density as derived from the AE-E Mesa experiment, *J. Geophys. Res.*, 84, 31-35, 1979.
- Hedin, A. E., H. G. Mayr, C. A. Reber, G. R. Carignan, and N. W. Spencer, A global empirical model of thermospheric composition based on Ogo-6 mass spectrometer measurements, *Space Res.*, 13, 315-320, 1973.
- Hedin, A. E., H. G. Mayr, C. A. Reber, N. W. Spencer, and G. R. Carignan, Empirical model of global thermospheric temperature and composition based on data from the Ogo-6 quadrupole mass spectrometer, *J. Geophys. Res.*, 79, 215-225, 1974.
- Hedin, A. E., A revised thermospheric model based on mass spectrometer and incoherent scatter data: MSIS-83, *J. Geophys. Res.*, 88, 10,170-10,188, 1983.
- Hedin, A. E., MSIS-86 thermospheric model, *J. Geophys. Res.*, 92, 4649-4662, 1987.
- Herrero, F. A., H. G. Mayr, and N. W. Spencer, Latitudinal (seasonal) variations in the thermospheric midnight temperature maximum: a tidal analysis, *J. Geophys. Res.*, 88, 7225-7235, 1983.
- Hinteregger, H. E., Representations of solar EUV fluxes for aeronautical applications, *Adv. Space Res.*, 1, 39-52, 1981.
- Hong, S. S., and R. S. Lindzen, Solar semidiurnal tide in the thermosphere, *J. Atmos. Sci.*, 28, 275-280, 1976.
- Jacchia, L. G., I. G. Campbell, and J. W. Slowey, A study of the diurnal variation in the thermosphere as derived by satellite drag, *Planet. Space Sci.*, 21, 1825-1834, 1973.
- Lindzen, R. S., On the relation of wave behavior to source strength and distribution in a propagating medium, *J. Atmos. Sci.*, 23, 630-632, 1966.

- Lindzen, R. S., and S. S. Hong, Effects of mean winds and horizontal temperature gradients on solar and lunar semidiurnal tides in the atmosphere, *J. Atmos. Sci.*, *31*, 1421-1466, 1974.
- Massey, H. S. W., and D. R. Bates, *Applied Atomic Collision Physics, Vol. 1, Atmospheric Physics and Chemistry*, 482 pp., Academic Press, New York, NY, 1982.
- Mayr, H. G., A. E. Hedin, C. A. Reber, and G. R. Carignan, Global characteristics in the diurnal variations of the thermospheric temperature and composition, *J. Geophys. Res.*, *79*, 619-628, 1974.
- Mayr, H. G., I. Harris, N. W. Spencer, A. E. Hedin, L. E. Wharton, H. S. Porter, J. C. G. Walker, and H. C. Carlson, Atmospheric tides and the midnight temperature anomaly, *Geophys. Res. Lett.*, *6*, 447-450, 1979.
- Mayr, H. G., and H. Volland, Diffusion model for the phase delay between thermospheric density and temperature, *J. Geophys. Res.*, *77*, 2359-2367, 1972.
- Newton, G. P., and H. G. Mayr, Diurnal and semidiurnal nitrogen density and temperature variations from thermosphere probe measurements, *J. Geophys. Res.*, *78*, 5687-5692, 1973.
- Newton, G. P., D. T. Pelz, and W. T. Kasprzak, Equatorial thermospheric composition and its variations, *Space Res.*, *13*, 287-290, 1973.
- Newton, G. P., W. T. Kasprzak, S. A. Curtis, and D. T. Pelz, Local time variation of equatorial thermospheric composition determined by the San Marco 3 NACE, *J. Geophys. Res.*, *80*, 2289-2299, 1975.
- Nier, A. O., W. E. Potter, D. R. Hickman, and K. Mauersberger, The open-source neutral-mass spectrometer on Atmosphere Explorer-C, -D, and -E, *Radio Sci.*, *8*, 271-276, 1973.
- Pelz, D. T., C. A. Reber, A. E. Hedin, G. R. Carignan, A neutral-atmosphere composition experiment for the Atmosphere Explorer-C, -D, and -E, *Radio Sci.*, *8*, 277-285, 1973.
- Rawer, K., *International Reference Ionosphere - IRI74*, Eds. J. V. Lincoln and R. O. Conkright, World Data Center A, NOAA, Boulder, CO, 1981.
- Robel, R. G., R. E. Dickinson, and E. C. Ridley, Global circulation and temperature structure of thermosphere with high-latitude plasma convection, *J. Geophys. Res.*, *87*, 1599-1614, 1982.
- Sharp, L. R., D. R. Hickman, C. J. Rice, and J. M. Straus, The altitude dependence of the local time variation of thermospheric density, *Geophys. Res. Lett.*, *5*, 261-263, 1978.
- Spencer, N. W., H. B. Niemann, and G. R. Carignan, The neutral-atmosphere temperature instrument, *Radio Sci.*, *8*, 284-296, 1973.
- Spencer, N. W., G. R. Carignan, H. G. Mayr, N. B. Niemann, R. F. Theis, and L. E. Wharton, The midnight temperature maximum in the earth's equatorial thermosphere, *Geophys. Res. Lett.*, *6*, 444-446, 1979.
- Volland, H., and H. G. Mayr, A theory of the diurnal variations of the thermosphere, *Ann. Geophys.*, *26*, 907, 1970.
- Wand, R. H., Semidiurnal tide in the E region from incoherent scatter measurements at Arecibo, *Radio Sci.*, *11*, 641-652, 1976.

Solar Tides in the Upper Equatorial Thermosphere:  
A Comparison Between AE-E Data and the NCAR  
Thermospheric General Circulation Model

by  
Mark F. Storz, Captain, USAF

This report (23 pages) was submitted  
as a requirement for the degree of  
Master of Science  
(Atmospheric Science)  
in the University of Michigan  
1987

# ~~Solar Tides in the Upper Equatorial Thermosphere : A Comparison Between AE-E Data and the NCAR Thermospheric General Circulation Model 1. Solstice~~

~~M. F. STORZ AND V. J. ABREU~~

~~*Space Physics Research Laboratory, Ann Arbor, Michigan*~~

~~C. G. FESEN~~

~~*Laboratory for Atmospheric and Space Physics, University of Colorado, Boulder, Colorado*~~

Numerical calculations of the equatorial thermospheric tidal temperatures and densities are compared with mass spectrometer data from the Atmosphere Explorer-E satellite (AE-E) for solar minimum solstice conditions. The model calculations were made using the National Center for Atmospheric Research thermospheric general circulation model (TGCM), which includes the effects of viscosity, conductivity, diffusion, ion drag, winds, and temperature gradients. The thermospheric diurnal and semidiurnal tides are excited in situ by solar heating and by ion-neutral momentum coupling. The semidiurnal tidal calculations also include the effects of upward propagating waves generated by heating in the lower atmosphere. The semidiurnal propagating component is modeled by use of the classical tidal perturbations as lower boundary conditions. The model has been tuned by adjusting the propagating tidal forcing term until calculated semidiurnal winds and temperature fields best approximate incoherent scatter observations. The TGCM reproduces the gross tidal features, including the nighttime maxima. The largest discrepancy is the relative weakness of the model's diurnal amplitudes. This may be due to uncertainties in the EUV heating rates and thermospheric cooling rates. On the other hand, the model semidiurnal density amplitudes are considerably larger than those of the data. The terdiurnal amplitudes match fairly well, but the data exhibit a greater asymmetry about the geographic equator.

## REFERENCES

- Broglia, L., C. Buongiorno, U. Ponzi, and G. Ravelli, San Marco 3 drag balance results below 320 km altitude in the equatorial atmosphere, *Space Res.*, 16, 203-207, 1976.
- Dickinson, R. E., C. P. Lagos, and R. E. Newell, Dynamics of the neutral thermosphere for small Rossby number motions, *J. Geophys. Res.*, 73, 4299-4313, 1968.
- Dickinson, R. E., E. C. Ridley, and R. G. Robel, A three-dimensional general circulation model of the thermosphere, *J. Geophys. Res.*, 86, 1499-1512, 1981.
- Dickinson, R. E., E. C. Ridley, and R. G. Robel, Thermospheric general circulation with coupled dynamics and composition, *J. Atmos. Sci.*, 41, 205-219, 1984.
- Fesen, C. G., R. E. Dickinson, R. G. Robel, Simulation of the thermospheric tides at equinox with the National Center for Atmospheric Research thermospheric general circulation model, *J. Geophys. Res.*, 91, 4471-4489, 1986.
- Fontanari, J., and D. Alcayde, Observations of neutral temperature tidal-type oscillations in the  $F_1$  region, *Radio Sci.*, 9, 275-280, 1974.
- Forbes, J. M., Atmospheric tides, 2, The solar and lunar semidiurnal components, *J. Geophys. Res.*, 87, 5241-5252, 1982.
- Forbes, J. M., and F. A. Marcos, Tidal variations in total mass density as derived from the AE-E Mesa experiment, *J. Geophys. Res.*, 84, 31-35, 1979.
- Hedin, A. E., H. G. Mayr, C. A. Reber, G. R. Carignan, and N. W. Spencer, A global empirical model of thermospheric composition based on Ogo-6 mass spectrometer measurements, *Space Res.*, 13, 315-320, 1973.
- Hedin, A. E., H. G. Mayr, C. A. Reber, N. W. Spencer, and G. R. Carignan, Empirical model of global thermospheric temperature and composition based on data from the Ogo-6 quadrupole mass spectrometer, *J. Geophys. Res.*, 79, 215-225, 1974.
- Hedin, A. E., A revised thermospheric model based on mass spectrometer and incoherent scatter data: MSIS-83, *J. Geophys. Res.*, 88, 10,170-10,188, 1983.
- Hedin, A. E., MSIS-86 thermospheric model, *J. Geophys. Res.*, 92, 4649-4662, 1987.
- Herrero, F. A., H. G. Mayr, and N. W. Spencer, Latitudinal (seasonal) variations in the thermospheric midnight temperature maximum: a tidal analysis, *J. Geophys. Res.*, 88, 7225-7235, 1983.
- Hinteregger, H. E., Representations of solar EUV fluxes for aeronautical applications, *Adv. Space Res.*, 1, 39-52, 1981.
- Hong, S. S., and R. S. Lindzen, Solar semidiurnal tide in the thermosphere, *J. Atmos. Sci.*, 28, 275-280, 1976.
- Jacchia, L. G., I. G. Campbell, and J. W. Slowey, A study of the diurnal variation in the thermosphere as derived by satellite drag, *Planet. Space Sci.*, 21, 1825-1834, 1973.
- Lindzen, R. S., On the relation of wave behavior to source strength and distribution in a propagating medium, *J. Atmos. Sci.*, 23, 630-632, 1966.

- Lindzen, R. S., and S. S. Hong, Effects of mean winds and horizontal temperature gradients on solar and lunar semidiurnal tides in the atmosphere, *J. Atmos. Sci.*, 31, 1421-1466, 1974.
- Massey, H. S. W., and D. R. Bates, *Applied Atomic Collision Physics, Vol. 1, Atmospheric Physics and Chemistry*, 482 pp., Academic Press, New York, NY, 1982.
- Mayr, H. G., A. E. Hedin, C. A. Reber, and G. R. Carignan, Global characteristics in the diurnal variations of the thermospheric temperature and composition, *J. Geophys. Res.*, 79, 619-628, 1974.
- Mayr, H. G., I. Harris, N. W. Spencer, A. E. Hedin, L. E. Wharton, H. S. Porter, J. C. G. Walker, and H. C. Carlson, Atmospheric tides and the midnight temperature anomaly, *Geophys. Res. Lett.*, 6, 447-450, 1979.
- Mayr, H. G., and H. Volland, Diffusion model for the phase delay between thermospheric density and temperature, *J. Geophys. Res.*, 77, 2359-2367, 1972.
- Newton, G. P., and H. G. Mayr, Diurnal and semidiurnal nitrogen density and temperature variations from thermosphere probe measurements, *J. Geophys. Res.*, 78, 5687-5692, 1973.
- Newton, G. P., D. T. Pelz, and W. T. Kasprzak, Equatorial thermospheric composition and its variations, *Space Res.*, 13, 287-290, 1973.
- Newton, G. P., W. T. Kasprzak, S. A. Curtis, and D. T. Pelz, Local time variation of equatorial thermospheric composition determined by the San Marco 3 NACE, *J. Geophys. Res.*, 80, 2289-2299, 1975.
- Nier, A. O., W. E. Potter, D. R. Hickman, and K. Mauersberger, The open-source neutral-mass spectrometer on Atmosphere Explorer-C, -D, and -E, *Radio Sci.*, 8, 271-276, 1973.
- Pelz, D. T., C. A. Reber, A. E. Hedin, G. R. Carignan, A neutral-atmosphere composition experiment for the Atmosphere Explorer-C, -D, and -E, *Radio Sci.*, 8, 277-285, 1973.
- Rawer, K., *International Reference Ionosphere - IRI74*, Eds. J. V. Lincoln and R. O. Conkright, World Data Center A, NOAA, Boulder, CO, 1981.
- Robel, R. G., R. E. Dickinson, and E. C. Ridley, Global circulation and temperature structure of thermosphere with high-latitude plasma convection, *J. Geophys. Res.*, 87, 1599-1614, 1982.
- Sharp, L. R., D. R. Hickman, C. J. Rice, and J. M. Straus, The altitude dependence of the local time variation of thermospheric density, *Geophys. Res. Lett.*, 5, 261-263, 1978.
- Spencer, N. W., H. B. Niemann, and G. R. Carignan, The neutral-atmosphere temperature instrument, *Radio Sci.*, 8, 284-296, 1973.
- Spencer, N. W., G. R. Carignan, H. G. Mayr, N. B. Niemann, R. F. Theis, and L. E. Wharton, The midnight temperature maximum in the earth's equatorial thermosphere, *Geophys. Res. Lett.*, 6, 444-446, 1979.
- Volland, H., and H. G. Mayr, A theory of the diurnal variations of the thermosphere, *Ann. Geophys.*, 26, 907, 1970.
- Wand, R. H., Semidiurnal tide in the E region from incoherent scatter measurements at Arecibo, *Radio Sci.*, 11, 641-652, 1976.

END

12-87

DTIC